Bull. Mater. Sci. (2018) 41:110
https://doi.org/10.1007/s12034-018-1615-1

Synthesis and luminescence properties of TiO_2 :Yb–Er mesoporous nanoparticles

I L VERA ESTRADA[1], R NARRO-GARCÍA[2], T LÓPEZ-LUKE[1], V H ROMERO[3,*], J A CHRISTEN[4] and E DE LA ROSA[1]

[1]Centro de Investigaciones en Óptica, A.P. 1-948, 37160 León, GTO, Mexico
[2]Facultad de Ingeniería, Universidad Autónoma de Chihuahua, Circuito Universitario S/N, 31125 Chihuahua, Chih., Mexico
[3]Centro Universitario de Tonalá, Universidad de Guadalajara, 48525 Tonalá, Jal., Mexico
[4]CIMAT, A.P. 402, 36000 Guanajuato, GTO, Mexico
*Author for correspondence (vicromare@gmail.com)

MS received 31 August 2017; accepted 27 November 2017; published online 27 July 2018

Abstract. Mesoporous spherical Yb–Er-doped TiO_2 nanoparticles were prepared by sol–gel method. The structure and morphology of the nanoparticles were characterized using Raman, Fourier transform infrared spectroscopies, transmission electron microscopy and by low-temperature N_2 adsorption. It is shown that both anatase (tetragonal) and brookite (orthorhombical) phases are present in the titania nanoparticles. Their diameter size is between 12 and 15 nm and an average surface area of 136 $m^2\ g^{-1}$. Under infrared irradiation, the nanoparticles show luminescence by an upconversion process of the ytterbium and erbium ions, the green emission corresponds to $^2H_{11/2} + {}^4S_{3/2} \rightarrow {}^4I_{15/2}$ transition and for the red emission, the transition energy is: $^4F_{7/2}$–$^4I_{15/2}$. The green and red photoluminescence intensities are highly dependent on the OH amount, which is produced during the hydrolysis and condensation processes and depends on the reaction time, nanoparticles wash and annealing temperature. The influence of synthesis parameters on the properties of porosity and luminescence was studied by the Plackett–Burman experimental design.

Keywords. Titanium; titanium dioxide; TiO_2:Yb–Er; mesoporous; luminescence; upconversion.

1. Introduction

The interesting and novel properties of the nanostructured materials have enabled a wide range of applications, which are from optic and electronics to medicine and biomedical devices [1]. The development of nanostructure materials with specific and controllable characteristics, such as size, morphology, crystalline structure and chemical composition, depends on the synthesis methods and processes in great measure [2,3]. One of the main features that can be determined by the synthesis process is the porosity. According to the International Union of Pure and Applied Chemistry (IUPAC), mesoporous materials have a pore size between 2 and 50 nm [4]. These materials have high surface area and volume, making them suitable for applications such as catalysis, separation of large molecules, photovoltaic cells, fuel cells, optical and electronic devices, encapsulation of proteins and diagnosis, and treatment of cancer [2,5,6].

Currently, the most studied mesoporous nanomaterial is the silicon oxide; because the silicon is an abundant element on Earth and because its oxide has very attractive properties [7,8]. However, research on other oxides such as alumina, circonia [9,10] and titania also started recently; the latter has received particular attention due to its excellent photoactivity, chemical stability and low toxicity [11,12].

Luminescence, besides porosity, is another attractive property of nanomaterials. Normally, these two properties are studied separately, however, nanomaterials with both properties are required for several applications. Generally, luminescence is obtained with the incorporation of rare earth ions such as Eu^{3+}, Er^{3+}, Yb^{3+}, etc. [13,14]; special attention was given to the upconversion luminescence process, in which the sequential absorption of two or more photons leads to the emission of light at shorter wavelength than the excitation wavelength. For this process, an appropriate matrix to host the doped ions is required. Titanium dioxide doped with rare earth seems to be a promising material for luminescence applications due to its high transparency in the visible range and its good chemical, thermal and mechanical properties, in addition to the advantage of its low cost.

There are some previous works about the applications of mesoporous TiO_2 doped with different rare earth ions [15–17], such as a scattering layer for dye-sensitized solar cells [18] or as photocatalyst due to its good activity to degrade different substances or microorganisms, such as *Aeromonas hydrophia* [19]. Other works on doped-TiO_2 nanoparticles are focussed on the luminiscence propierties, for example, Jianbo

Table 1. Plackett–Burman design for 12 runs and 11 two-level factors.

No.	X_1 (ml)	X_2 (ml)	X_3 (g)	X_4 (h)	X_5 (°C)	X_6 (h)	X_7 (ml)	X_8	X_9	X_{10} (°C)	X_{11} (ml)
S1	60	9	8.5	9	35	0	0.3	End	Wash	400	13
S2	60	160	1.5	16	35	0	0	End	Wash	500	8
S3	5	160	8.5	9	85	0	0	Beginning	Wash	500	13
S4	60	9	8.5	16	35	1	0	Beginning	Dry	500	13
S5	60	160	1.5	16	85	0	0.3	Beginning	Dry	400	13
S6	60	160	8.5	9	85	1	0	End	Dry	400	8
S7	5	160	8.5	16	35	1	0.3	Beginning	Wash	400	8
S8	5	9	8.5	16	85	0	0.3	End	Dry	500	8
S9	5	9	1.5	16	85	1	0	End	Wash	400	13
S10	60	9	1.5	9	85	1	0.3	Beginning	Wash	500	8
S11	5	160	1.5	9	35	1	0.3	End	Dry	500	13
S12	5	9	1.5	9	35	0	0	Beginning	Dry	400	8

X_1 = water amount, X_2 = alcohol amount, X_3 = surfactant amount, X_4 = reaction time, X_5 = reaction temperature, X_6 = N_2 atmosphere exposure time, X_7 = nitric acid, X_8 = addition order of surfactant, X_9 = wash/dry treatment, X_{10} = annealing temperature, X_{11} = precursor amount.

Yin *et al* [13] have shown that mesoporous monodispersed titania doped with Eu^{3+} shows a strong red emission under UV radiation. The objective of present work was to get luminescence by the phenomenon of upconversion by sintering Yb–Er co-doped mesoporus TiO_2 nanoparticles.

Mesoporous and luminescent nanoparticles studies show that several synthesis parameters affect these two properties in different ways [10,12–14,20,21]. Therefore, it is important to establish an optimum process that allows mesoporous nanoparticles to have good luminescent properties. For this purpose, it was established a synthesis process, where different factors were studied at two different levels or states; given the high number of possible synthesis paths, a fractional factorial experiment design of the Placket–Burmann type was choosen [22,23]. Finally, the results were evaluated by a linear regression model to find the main factors that can affect the principal mesoporous and luminescent characteristics, such as pore size, surface area and photoluminscense intensity.

2. Experimental

2.1 *Chemicals and titanium dioxide nanoparticles synthesis*

All the chemicals were used as received without further purification. Titanium tetrabutoxide ($C_{16}H_{36}O_4Ti$, purity > 97%), ytterbium (III) chloride hexahydrate ($YbCl_3 \cdot 6H_2O$, purity > 99.998%) and Pluronic F127 $(C_3H_6O \cdot C_2H_4O \cdot C_3H_6O)_x$ were obtained from Sigma-Aldrich. Erbium (III) chloride hexahydrate ($ErCl_3 \cdot 6H_2O$, purity > 99.99%) was obtained from Alfa Aesar company. Distilled water (H_2O, purity > 99.5%) was used throughout the experiment.

Titanium dioxide nanoparticles were synthesized by a modified sol–gel method adapted from the literature [11,13]. In general, this process is as follows: titanium tetrabutoxide (8 or 13 ml), erbium (III) chloride hexahydrate (2%) and ytterbium (III) chloride hexahydrate (1%) are dissolved in isopropyl alcohol (9 or 160 ml). For some samples, the surfactant (Pluronic F127) is added (1.5 or 8.5 g) at this stage of the process (addition order of surfactant = beginning). Then, the nitric acid (0 or 0.3 ml) is added to the solution. Then, water (5 or 60 ml) is added to the solution and with this, the hydrolysis and condensation reactions begin (1–3). This solution must be kept for 9 or 16 h with a constant temperature (35 or 85°C), stirring and refluxing. During this step, the solution was kept under N_2 atmosphere by 1 or 0 h. For some samples, the surfactant is added after this step of the process (addition order of surfactant = end). In this case, the temperature is previously reduced to 35°C. With these new conditions, the reaction is kept for three more hours under stirring. Then, a wash or dry treatment is carried out. In the wash treatment, the gel obtained is washed and centrifuged with ethanol two times. For the dry treatment, the gel obtained is dried at 60°C in a ceramic crucible for 48 h. The product was subsequently annealed at the indicated temperature (400 or 500°C) for 4 h. Finally, the nanoparticles obtained were ground in an agate mortar. Specific conditions for synthesis of each sample are presented in table 1.

Hydrolysis:

$$\equiv \mathrm{Ti{-}(OR)} + \mathrm{H_2O} \Leftrightarrow \equiv \mathrm{Ti{-}OH} + \mathrm{ROH}. \quad (1)$$

Condensation:

$$\equiv \mathrm{Ti{-}O} + \mathrm{OH{-}Ti} \equiv \Leftrightarrow \equiv \mathrm{Ti{-}O{-}Ti} \equiv + \mathrm{ROH}. \quad (2)$$

$$\equiv \mathrm{Ti{-}OH} + \mathrm{HO{-}Ti} \equiv \Leftrightarrow \equiv \mathrm{Ti{-}O{-}Ti} \equiv + \mathrm{H_2O}. \quad (3)$$

R represents butil($CH_3CH_2CH_2CH_2$–).

2.2 *Structural, morphological and photoluminescence characterization*

Raman spectra were obtained using a disperse Raman microscope spectrometer (Senterra model). The samples were excited with a 785 nm laser. The integration time of each Raman measurements was 10 s. The Fourier transform infrared (FTIR) spectra were obtained using a Spectrum BX spectrophotometer from Perkin–Elmer with a triglycine sulfate detector (DTGS) at 4 cm^{-1} spectral resolution and Beer–Norton anodization; measurements were performed in the attenuated total reflectance (ATR) mode using 100 mg of nanophosphor covering the whole active area of the ATR device. The spectra were obtained in the medium-infrared region from 1000 to 4000 cm^{-1} with 20 scans per spectra.

Transmission electron microscopy (TEM) images were collected on a Tecnai G2 F30 S-Twin TEM at 300 kV. The microscope is equipped with a Schottky-type field emission gun and an S-Twin objective lens (Cs = 1.2 mm; Cc = 1.4 mm; point to point resolution, 0.20 nm). Nitrogen adsorption–desorption isotherms were collected at 77 K using a Digisorb 2600 equipment. Specific surface areas were determined by the Brunauer–Emmett–Teller (BET) method. Pore size distribution was calculated from the N_2 isotherm at 77 K based on the Barret–Joyner–Halenda (BJH) model.

Photoluminescence (PL) characterization was performed using a CW semiconductor laser diode with a 350 mW pumping source centred at 980 nm. The PL was analysed with a Spectrograph SpectraPro 2300i. The system was PC controlled with Spectra-Sense software. All measurements were done at room temperature. Sample's pellets were made with 0.25 g of the nanoparticles and were pressed with 0.5 ton for 4 min, this guarantees the same quantity of excited material, better intensity of the sample and also eliminates possible interference. Special care was taken to maintain the alignment of the setup to compare the intensity of the upconverted signal between different characterized samples.

3. Theory

3.1 *Plackett–Burmann design and analysis*

Table 1 shows the Plackett–Burmann experimental design used to investigate the dependence of the pore size diameter (φ), surface area (s) and green (α), red (β) and overall (γ) PL intensity of the titanium dioxide nanoparticles on: (X_1) water amount (ml); (X_2) alcohol amount (ml); (X_3) surfactant amount (g); (X_4) reaction time (h); (X_5) reaction temperature (^{o}C); (X_6) N_2 atmosphere exposure time (h); (X_7) nitric acid amount (ml); (X_8) addition order of surfactant (end and beginning); (X_9) wash/dry treatment; (X_{10}) annealing temperature (°C); and (X_{11}) titanium tetrabutoxide amount (ml). Each factor was studied at two different levels or states [22].

The pore size diameter, the superficial area and the PL intensity (red, green and overall intensities) were individually analysed by a multiple lineal regression model (4–8). The parameters a_j, b_j, c_j, d_j and e_j; where $j = 0, 1, 2, \ldots, 11$ are called the regression coefficients. This model describes a hyper-plane in the 11-dimensional space of the studied factors X_j. The regression coefficients represent the expected change in response ($\varphi, s, \alpha, \beta, \gamma$) per unit change in X_j when all the remaining independent variables X_k ($k \neq j$) are held constant and the sign of the coefficient determines whether the influence is direct or inverse; i.e., the sign is interpreted as an increase or decrease of the surface area, pore size and intensity of luminescence [24].

$$\varphi_i = a_0 + a_1 X_{i1} + a_2 X_{i2} + \ldots + a_{11} X_{i11}, \quad (4)$$

$$s_i = b_0 + b_1 X_{i1} + b_2 X_{i2} + \ldots + b_{11} X_{i11}, \quad (5)$$

$$\alpha_i = c_0 + c_1 X_{i1} + c_2 X_{i2} + \ldots + c_{11} X_{i11}, \quad (6)$$

$$\beta_i = d_0 + d_1 X_{i1} + d_2 X_{i2} + \ldots + d_{11} X_{i11}, \quad (7)$$

$$\gamma_i = e_0 + e_1 X_{i1} + e_2 X_{i2} + \ldots + e_{11} X_{i11}, \quad (8)$$

$i = 1, 2, \ldots, 12.$

4. Results

4.1 *Structural characterization*

Figure 1 shows the Raman spectra of TiO_2:Yb–Er nanoparticles annealed at (a) 500 and (b) 400°C. The Raman spectra show that the titania nanoparticles present two crystalline phases: anatase (tetragonal) and brookite (orthorhombical) phases. Figure 1a shows four high peaks centred at 146.5, 398, 517.5 and 641 cm^{-1}. According to the group theory [25], these four peaks can be assigned as the Eg, B1g, A1g or B1g, and Eg modes of the anatase phase, respectively. Figure 1b shows the same modes of the anatase phase and an additional low peak at 323 cm^{-1} that could be assigned to the brookite (orthorhombical) phase [26]. It is known that the atomic radii of ytterbium and erbium are close; however, they are different with respect to titanium. The coordination of Yb and Er ions in doped-TiO_2 was not fully resolved; however, previous reports demonstrated that the La^{3+} ions can replace Ti^{4+} ion in TiO_2 [27], then, we assume that without more evidence, Yb^{3+} and Er^{3+} ions are likely to occupy the Ti^{4+} sites within TiO_2, because the ionic radii difference between Yb^{3+}/Er^{3+} (0.086, 0.089 nm, respectively) and Ti^{4+} (0.068 nm) is smaller than that of between Ti^{4+} (0.068 nm) and La^{3+} (0.1016 nm), as assumed in other works also [28].

Figure 2 shows the infrared spectra of TiO_2:Yb–Er nanoparticles. For a better clarity, only samples S2, S10 and S11 are shown. The wavenumber of the spectra ranges from 400 to 4000 cm^{-1}. All spectra show four different peaks.

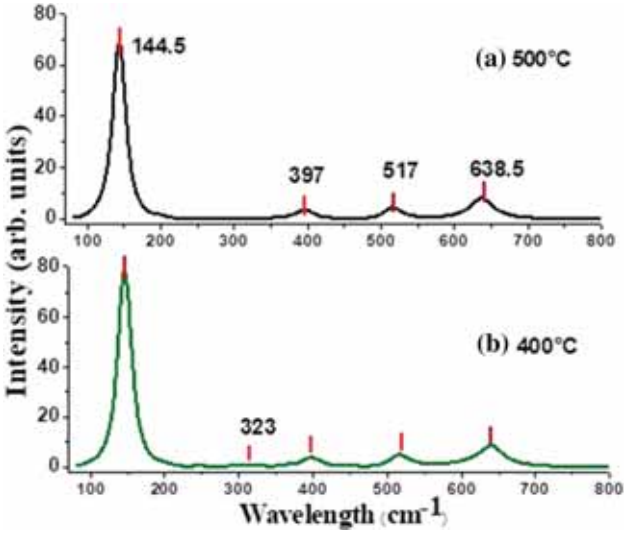

Figure 1. Raman spectra of TiO_2:Yb–Er nanoparticles annealed at different temperatures: (**a**) 400 and (**b**) 500°C.

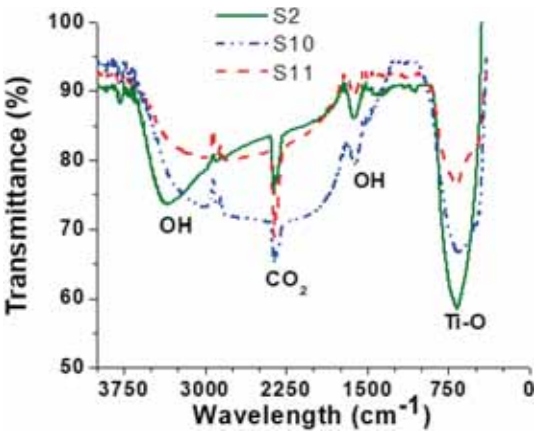

Figure 2. FTIR spectra of TiO_2:Yb–Er nanoparticles.

The peak situated at 650 cm^{-1} is attributed to the stretching vibration of Ti–O bonds. The peak at 1600 cm^{-1} corresponds to the bending vibrations of the O–H bond of chemisorbed water. The peak at 2300 cm^{-1} is associated with CO_2 adsorbed to the surface, partly from the synthesis and partly from the environment during the measurement process. The peak within 3000–3700 cm^{-1} is attributed to the hydroxyl groups that may come from the remaining alcohol and/or water. It is worth to note that the –OH vibration was reduced for sample S11, which implies that –OH groups on the nanoparticles surface were efficiently reduced.

4.2 *Morphological characterization*

Figure 3a shows a representative TEM image of TiO_2:Yb–Er mesoporous nanoparticles. The TEM image shows that the nanoparticles are well dispersed. The particle size distribution was evaluated by measuring hundreds of particles and it is reported in figure 3b. The average size of the nanoparticles ranges from 12 to 15 nm.

The adsorption–desorption isotherms of TiO_2:Yb–Er nanoparticles are shown in figure 4 and their BET specific surface areas and pore size diameter are listed in table 2. As shown in figure 4, all isotherms are identified as type IV, which are typical characters of mesoporous materials [29]. It is observed that samples S1–S5, S7, S9 and S11 present a H1 hysteresis loop at relative pressure of 0.5–1, while samples S6, S8 and S12 present H3 hysteresis loop. The BET analysis shows that the pore size diameter is between 6.5 and 23 nm with the surface area between 99 and 173 $m^2\ g^{-1}$.

4.3 *Lineal model analysis for mesoporous nanoparticles*

The sign of each coefficient (a_j, b_j) was found by substituting the pore size diameter and the specific surface area from table 2 and the factor levels from table 1 in equations (4) and (5). It was observed that alcohol and precursor amount have an inverse effect on the pore size. On the other hand, the reaction temperature and annealing temperature have a direct effect. Regarding the specific surface area, water amount, the reaction time, the reaction temperature, presence of N_2 atmosphere, addition of the surfactant at the end of the process and the nanoparticles washing have a direct effect on the surface area. On the other hand, absence of nitric acid, annealing temperature and precursor amount have an inverse effect on the surface area (see table 3).

4.4 *Luminescence properties*

Figures 5 and 6 show the upconversion emission spectra of the TiO_2:Yb–Er annealed at 400 and 500°C. The spectra show two emission bands at 560 and 660 nm. It is observed that the upconversion emission intensity depends on several factors, but the annealing temperature was the dominant factor. Green and red weak emissions were observed in the samples annealed at 400°C. On the other hand, the upconversion emission of the samples annealed at 500°C is higher than the samples annealed at 400°C (see figures 5 and 6). A quantification of the green, red and overall integrated intensities is presented in figure 7a. The highest green and red emissions correspond to samples S3 and S10, respectively. The green and red PL intensity is highly dependent on the OH amount, which is produced during the hydrolysis and condensation process and depends on the water amount and annealing temperature**.** If higher the water amount in the synthesis, higher the amount of OH groups in the surface of nanoparticles. These OH groups produce high-energy vibrational modes (3200–3800 cm^{-1}), which could enhance the red band by the phonon coupling of $^4F_{7/2} \rightarrow {}^4F_{9/2}$ and $^4I_{11/2} \rightarrow {}^4I_{13/2}$ transitions (see figure 8) as was observed previously in ZrO_2 nanocrystals [10]. To highlight the effect of water amount on the green and red emissions, the red/green ratio is plotted in figure 7b. It is observed that in the samples synthesized with a low water amount, the average R/G ratio is 1.13, but for

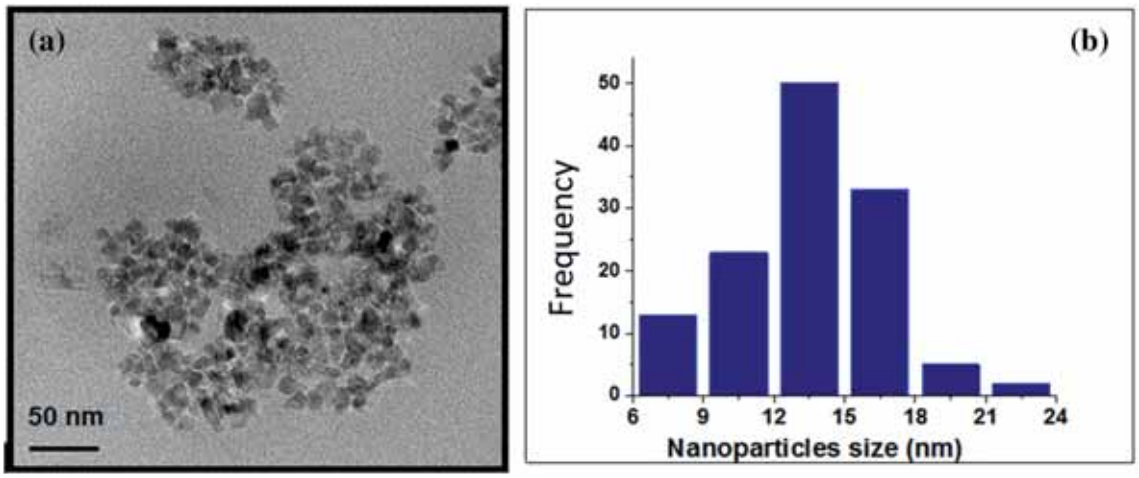

Figure 3. (**a**) TEM image of TiO_2:Yb–Er mesoporous nanoparticles and (**b**) particle size distribution.

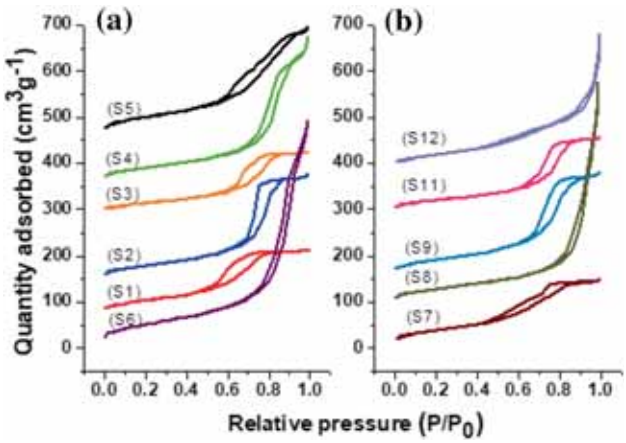

Figure 4. Nitrogen adsorption–desorption isotherms of TiO_2:Yb–Er nanoparticles.

Table 2. Pore size and surface area of TiO_2:Yb–Er nanoparticles.

Sample no.	Pore size diameter (nm)	Specific surface area ($m^2\ g^{-1}$)
S1	6.6358	137.06
S2	10.714	136.26
S3	8.6141	99.025
S4	14.698	133.23
S5	9.4248	156.55
S6	17.2	173.36
S7	6.5942	137.91
S8	23.835	125.62
S9	9.5663	146.72
S10	10.2568	135.60
S11	9.7801	103.22
S12	11.799	135.23

Table 3. Results of the lineal model for the specific pore size and surface area effects.

Studied factor	Pore size effect	Surface area effect
Alcohol amount	Inverse	N/A
Water amount	N/A	Direct
Reaction time	N/A	Direct
Reaction temperature	Direct	Direct
N_2 atmosphere exposure time	N/A	Direct (with)
Nitric acid	N/A	Inverse (without)
Addition order of surfactant	N/A	Direct (end)
Nanoparticles washing	Inverse	Direct
Annealing temperature	Direct	Inverse
Precursor amount	Inverse	Inverse

N/A: not applicable.

higher water amount, the average R/G ratio is increased to 3, indicating that samples with higher water amount favours the red emission. It was noted that besides water amount and annealing temperature, the green and red emissions depend also on the reaction time and nanoparticles wash, and it was concluded that a specific combination of the states or values of these four factors must be fulfilled to achieve the maximum green or red emissions. The relation of these states with the green and red emissions are shown in table 4.

These visible emission bands resulted from the well-known upconversion process. In this process (see figure 8), Er^{3+} from the ground state ($^4I_{15/2}$) is excited first to the $^4I_{11/2}$ level through one of the following processes: ground state absorption (GSA): $^4I_{15/2}$ (Er^{3+}) + a photon → $^4I_{11/2}$ (Er^{3+}); energy transfer (ET) from Yb^{3+} ($^2F_{5/2}$) state (ET_1): $^2F_{5/2}$ (Yb^{3+}) + $^4I_{15/2}$ (Er^{3+}) → $^2F_{7/2}$(Yb^{3+})+$^4I_{11/2}$ (Er^{3+}); and ET from the $^4I_{11/2}$ state of adjacent Er^{3+}. Among these three processes, ET from Yb^{3+} is most probable due to the larger absorption cross-section of Yb^{3+} at 980 nm. After the excitation at $^4I_{11/2}$ state, further excitation at $^4F_{7/2}$ state takes place either of the three following processes: (1) excited state absorption (ESA_1) $^4I_{11/2}$(Er^{3+}) + a photon → $^4F_{7/2}$ (Er^{3+});

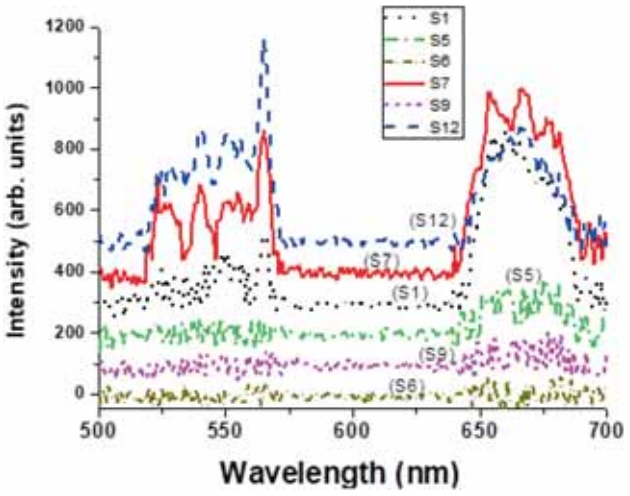

Figure 5. Upconversion emission spectra for the TiO_2:Yb–Er samples (S1, S5, S6, S7, S9 and S12) annealed at 400°C. (Curves were displaced 100 units to each other, for better visualization).

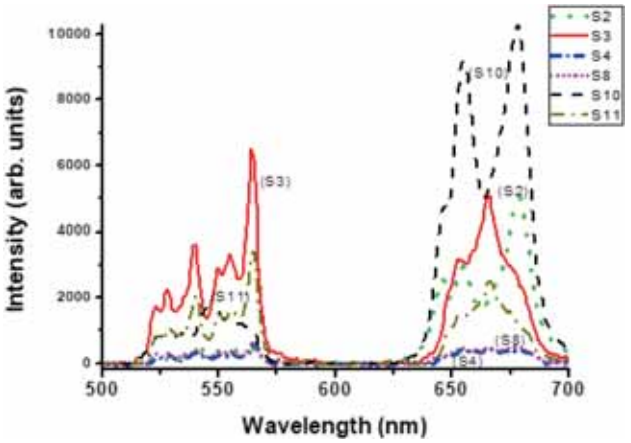

Figure 6. Upconversion emission spectra for the TiO_2:Yb–Er samples (S2, S3, S4, S8, S10 and S11) annealed at 500°C.

(2) ET_2 from Yb^{3+}, $^2F_{5/2}(Yb^{3+}) + {}^4I_{11/2}$ $(Er^{3+}) \rightarrow {}^2F_{7/2}(Yb^{3+}) + {}^4F_{7/2}(Er^{3+})$; and (3) ET from the $^4I_{11/2}$ state of adjacent Er^{3+}, $^4I_{11/2}(Er^{3+}) + {}^4I_{11/2}(Er^{3+}) \rightarrow {}^4F_{7/2}(Er^{3+}) + {}^4I_{15/2}(Er^{3+})$, in the last case, the ET mechanism promotes one Er^{3+} ion populated at $^4I_{11/2}$ to the higher level $^4F_{7/2}$, while a neighbouring Er^{3+} ion also populated at $^4I_{11/2}$ is taken back to the ground state. Populated $^4F_{7/2}$ state may undergo nonradiative relaxation to the $(^2H_{11/2} + {}^4S_{3/2})$ intermediate state through multiphonon relaxation process and finally, the transition from the $(^2H_{11/2} + {}^4S_{3/2}) \rightarrow {}^4I_{15/2}$ state results in the green emission around 550 nm. Similarly, Er^{3+} ion at the $^4F_{7/2}$ state can also decay rapidly down to the $^4F_{9/2}$ state, and finally the $^4F_{9/2} \rightarrow {}^4I_{15/2}$ transition reveals red emissions. Moreover, population at $^4I_{13/2}$ state could be promoted to the $^4F_{9/2}$ state by one of the two following processes: (1) ESA_2, $^4I_{13/2}$ (Er^{3+}) + photon $\rightarrow {}^4F_{9/2}$ (Er^{3+}); and (2) ET_3 from Yb^{3+}, $^2F_{5/2}$ $(Yb^{3+}) + {}^4I_{13/2}(Er^{3+}) \rightarrow {}^2F_{7/2}$ $(Yb^{3+}) + {}^4F_{9/2}(Er^{3+})$.

4.5 *Lineal model analysis for luminescence nanoparticles*

The PL intensity (green, red and overall intensities) was analysed by a lineal regression model (6–8). The sign of each coefficient (c_j, d_j and e_j) was found when substitution of the green, red and overall intensity values from figure 7a and the factor levels from table 1 in equations (6)–(8).

It was observed that water amount and the reaction time have an inverse effect on the green intensity, while the annealing temperature has a direct effect (table 4). In the case of red emission, the lineal regression model indicates that the water amount, nanoparticles wash and annealing temperature have a direct effect, while the reaction time has an inverse effect. Finally, in the case of overall intensity, it was observed that the nanoparticles wash and annealing temperature have a direct

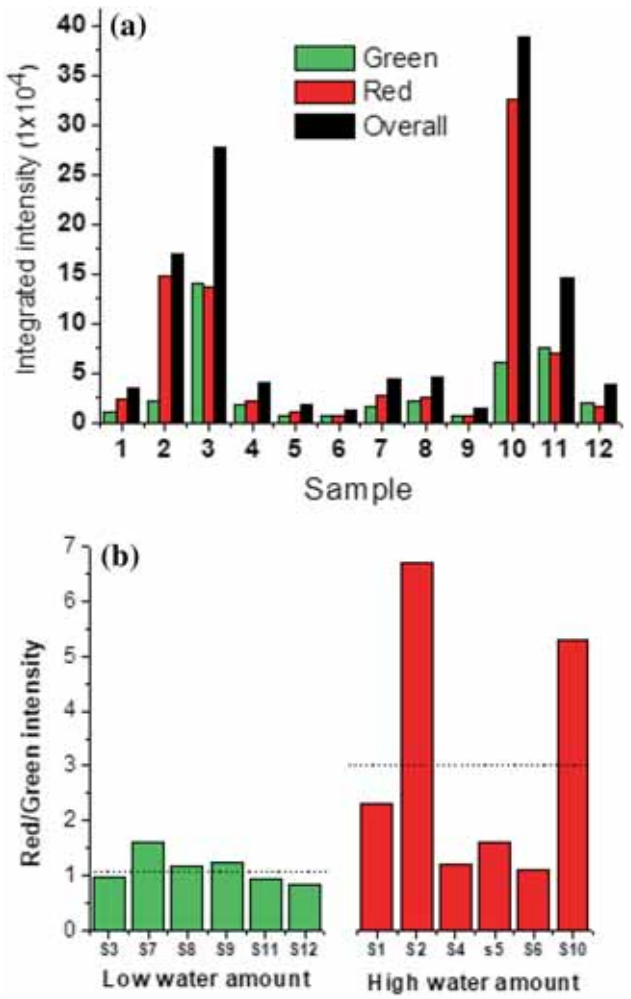

Figure 7. (**a**) Green, red and overall integrated intensities of the TiO_2:Yb–Er nanoparticles and (**b**) green/red ratio for samples with low (S3, S7, S8, S9, S11 and S12) and high (S1, S2, S4, S5, S6 and S10) water amounts.

Table 4. Results of the lineal model analysis for the photoluminescence intensity.

Factor	Effect		
	Green	Red	Green and red
Water amount	Inverse	Direct	N/A
Reaction timetime	Inverse	Inverse	Inverse
Nanoparticles wash	Direct	Direct	Direct
Annealing temperature	N/A	Direct	Direct

N/A: not applicable.

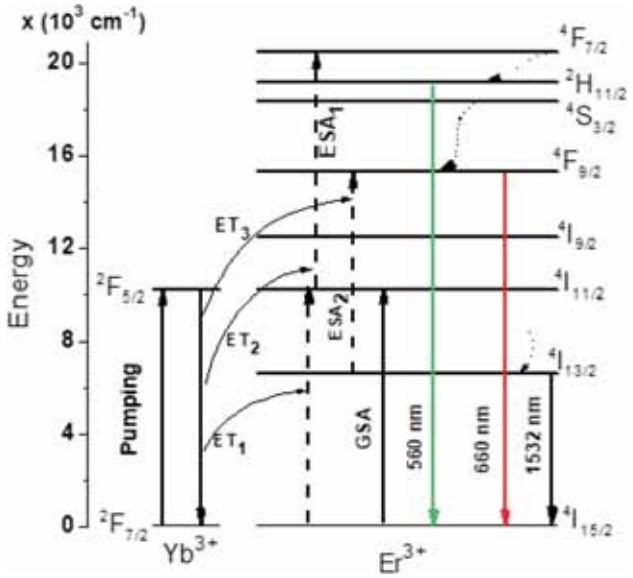

Figure 8. Energy-level diagram for the upconversion process of TiO_2:Yb–Er nanoparticles.

effect, while the reaction time has an inverse effect. It can be concluded from the latter results that the green and red PLs are also highly dependent on the water amount, which affects directly to the OH amount. Hence, higher the water amount in the synthesis, higher the amount of OH groups in the surface of the nanoparticles. These OH groups produce high-energy vibrational modes (3200–3800 cm^{-1}), which could enhance the red band by the phonon coupling of $^4F_{7/2} \rightarrow {}^4F_{9/2}$ and $^4I_{11/2} \rightarrow {}^4I_{13/2}$ transitions (see figure 8) as was observed previously in ZrO_2 nanocrystals [10].

5. Conclusions

The sol–gel method was used to synthesize mesoporous-luminesecent nanoparticles. The Raman spectra show that the titania nanoparticles present two crystalline phases: the anatase (tetragonal) and the brookite (orthorhombical) phases. The TEM images show that the average size of the nanoparticles ranges from 12 to 15 nm. The BET analysis showed that nanoparticles pore size diameter is between 6.5 and 23 nm with 10 nm as an average and that the specific surface area is between 99 and 156 $m^2\ g^{-1}$, which was sensitive (direct or inverse) to various factors involved during synthesis, such as the reaction temperature, nanoparticles washing, annealing temperature, etc. The ytterbium–erbium co-doped nanoparticles showed green and red emissions under 980 nm as a result of the upconversion process. The green and red photoluminescence intensities are highly dependent on the OH amount, which is produced during the hydrolysis and condensation processes and depends on the reaction time, nanoparticles wash and annealing temperature. In this work, we studied the synthesis of nanoparticles that were mesoporous and luminescent at the same time; as was mentioned before, it has shown that both characteristics depend on several synthesis factors. It was also identified, if the effect of those factors was direct or inverse on the studied variables (i.e., pore size, surface area and luminescence) and it was found that in some cases, these factors contribute in opposite ways to the desired characteristics (mesoporosity and luminescence). Thus, it can be concluded that special conditions are necessary to synthesize mesoporous luminescent nanoparticles, which could be used in several applications in future.

Acknowledgements

Authors acknowledge financial support to CONACYT grant 259192, LANIAUTO (294030), and CIMIE-SOLAR (207450) consortium projects P27 and P28.

References

[1] Holister P, Willem Weener J, Román Vas C and Harper T 2003 *Científica* **3** 5
[2] López-Luke T, De La Rosa E, Romero V H, Ángeles-Chávez C and Salas P 2010 *Appl. Phys. B* **102** 641
[3] Peng L, Tang A-W, Jia Y, Pan L and Zou J-J 2017 *Sci. Adv. Mater.* **9** 782
[4] McNaught A D and Wilkinson A 1997 *Compendium of chemical terminology* (Oxford: Blackwell Scientific Publications)
[5] Ozin G A and Arsenault A C 2006 *Nanochemistry: a chemical approach to nanomaterials* (Cambridge: RSC Publishing)
[6] Scott B J, Wirnsberger G and Stucky D 2001 *Chem. Mater.* **13** 3140
[7] Antonietti M 2003 *Topics in current chemistry: colloid chemistry I* (Germany: Springer)
[8] Dai Y, Shen S, Ma Z, Ma L, Sun Z, Yu J *et al* 2017 *J. Nanosci. Nanotechnol.* **17** 3772
[9] Quezada J C, Villaquiran C F, Scian A and Rodríguez-Páez J E 2006 *Rev. Latin Am. Metal. Mater.* **26** 95
[10] Solís D, López-Luke T, De la Rosa E, Salas P and Angeles-Chavez C 2009 *J. Lumin.* **129** 449
[11] Bleta R, Alphonse P and Lorenzato L 2010 *J. Phys. Chem. C* **114** 2039

[12] Benkacem T and Agoudjil N 2008 *Am. J. Appl. Sci.* **5** 1437
[13] Yin J, Xiang L and Zhao X 2007 *Appl. Phys. Lett.* **90** 113112
[14] Cao B S, He Y Y, Feng Z Q, Song M and Dong B 2011 *Opt. Commun.* **284** 3311
[15] Stengl V, Bakardjieva S and Murafa M 2009 *Mater. Chem. Phys.* **114** 217
[16] Shi H, Zhang T and Wang H 2011 *J. Rare Earth* **29** 746
[17] Feng G, Liu S, Xiu Z, Zhang Y, Yu J, Chen Y *et al* 2008 *J. Phys. Chem. C* **112** 13692
[18] Han C-H, Lee H-S, Lee K-W, Han S-D and Singh I 2009 *B. Korean Chem. Soc.* **30** 219
[19] Wang W, Shang Q, Zheng W, Yu H, Feng X, Zhang Y *et al* 2010 *J. Phys. Chem. C* **114** 13663
[20] Chen D, Huang F, Cheng Y-B and Caruso R A 2009 *Adv. Mater.* **21** 2206
[21] Romero V H, De La Rosa E and Salas P 2010 *Sci. Adv. Mater.* **4** 551
[22] Gutiérrez Pulido H and De la Vara Salazar R 2008 *Análisis y diseño de experimentos* (DF: McGraw Hill)
[23] Plackett R L and Burman J P 1946 *Biometrika* **33** 305
[24] Novakovic T B, Rozic L S, Petrovic Z M and Mitric M N 2015 *J. Serb. Chem. Soc.* **80** 1
[25] Ohsaka T 1980 *J. Phys. Soc. Jpn.* **48** 1661
[26] Hu Y, Tsai H L and Huang C L 2003 *J. Eur. Ceram. Soc.* **23** 691
[27] Sibu C P, Rajesh Kumar S, Mukundan P and Warrier K G K 2002 *Chem. Mater.* **14** 2876
[28] Yang Z, Zhu K, Song Z, Zhou D, Yin Z and Qiu J 2011 *Solid State Commun*. **151** 364
[29] Schmidt R, Stöcker M, Hansen E, Akporiaye D and Ellestad O H 1995 *Micropor. Mat.* **3** 443